Dynamics of films and droplets spreading on porous substrates

NORBERT ALLEBORN AND HANS RASZILLIER

ABSTRACT: This paper numerically investigates spreading and sorption of films and droplets on an unsaturated porous substrate, a mechanism taking place in paper coating and ink jet printing. The dynamics of the fluid on the substrate surface are described by lubrication approximation. Fluid flow within the porous substrate, caused by the droplet penetrating into it, is treated with the Richards' equation, which models unsaturated flow in porous media and describes fluid transport in the porous layer after complete absorption of the film or droplet. Numerical results for sorption of an axisymmetric droplet into a substrate of finite thickness show that a sharp localization of the penetrating fluid, as required for fine printing resolution, can be achieved by a steep capillary sorption curve. The interaction of the fluid with the impermeable bottom of the layer may drastically delay droplet absorption and thus require matching layer thickness and droplet volume to avoid limiting printing process speed.

Application: The numerical model gives insight into how the sorption properties of the porous receiving layer and its thickness influence absorption time, which limits printing speed, and fluid distribution, which determines print resolution.

The processes of spreading and sorption of droplets on unsaturated porous substrates are relevant in ink-jet printing [1-3] and in micro-fabrication of ceramic structures [4]. Penetration of liquid films into porous substrates plays an important role during levelling of pigmented films of coating color in paper coating processes [5-7], in printing [8], and in coating of solid porous materials [9]. The absorption kinetics of a film or droplet on top of the porous substrate limits the speed for coating and post-processing of the substrate. The fluid distribution within a porous material, and possibly its continuing migration due to capillary forces after complete absorption of the liquid into the porous material, crucially influence the quality of the coated product.

Spreading of a droplet and its penetration into porous substrates has been covered in numerous publications; for infinitely thick substrates [10, 11] and for layered substrates [12, 13]. In those papers, the droplet dynamics are treated in the framework of lubrication approximation. A wetting front model is employed in the porous layers, assuming a sharp transition from fully saturated to completely unsaturated regions.

In the context of paper coating, penetration of the water phase into complex three-dimensional interconnected pore structures has been investigated by Bousfield and Karles [14] and Schoelkopf et al. [8], using pore network models. The pore network model [8, 15] allows simulation of the void space structure of porous materials such as sandstone, medical tablets, and compacted blocks of coating pigments. Cubic pores are arranged in a three-dimensional array and connected by cylindrical [15] or conical [16] throats. The pore and throat size distribution are optimized so that the simulated percolation curve matches experimental data [8]. The model gives valuable insight into physical mechanisms of liquid absorption in complex pore networks, such as the interplay of inertial and viscous forces [15, 17] or the effect of void geometry [16], and their implications on the characterization of porous materials by experimental methods [8, 17]. Practical guidelines were derived for a systematically optimized design of coating pigments [18].

Gillespie [19], in a study of penetration of liquid droplets into thin paper substrates, identified two phases of spreading. During phase 1 some liquid remains on top of the paper substrate and forms a flat droplet. In phase 2, spreading takes place entirely in the substrate, with no fluid outside the substrate. During phase 2, the flow in the porous layer is unsaturated (i.e., the void space may not be completely filled with fluid locally) and driven by capillary forces, described by Richards' equation [20].

While the wetting front model describes the interplay between droplet dynamics and penetration [2, 10, 13, 21, 22], phase 2 sorption is beyond its reach because the advance of the wetting front will cease upon complete absorption of the droplet, simply due to mass conservation for an incompressible fluid. The wetting front model approximates a porous material with narrow pore size distribution, essentially representing the limiting case of a single pore radius [12, 23, 24].

For materials with a broad pore size distribution and possibly nonhomogeneous properties, a continuous transition from fully saturated to completely unsaturated regions will take place over a finite distance.

In our paper we modelled unsaturated flow in the porous layer with a continuum approach, using Richards' equation, coupled with the droplet dynamics described by lubrication approximation. We describe the geometry, material, and operation conditions of the problem and the governing equations and boundary conditions for droplet dynamics and flow in the porous layer. We also present results of numerical computations for the imbibition of a droplet into substrate layers with three different sorption characteristics and different layer thicknesses and discuss their implications for the sorption process.

PROBLEM FORMULATION

When applying a thin liquid film onto a porous substrate, the lateral extent of the film and the lateral length scale of film thickness variations (perturbations) are generally large compared with the film thickness, introducing two length scales and making the problem amenable to asymptotic analysis. During droplet application, impact and dissipation of kinetic energy takes place in a very short time [3, 4]. At the end of this short impingement phase, capillary phenomena dominate the dynamics of spreading and sorption and the droplet has a shape similar to a flat spherical cap. If the fluid also wets the substrate with a small equilibrium contact angle, the flatness of the droplet allows treating the flow in the droplet, like the flow in a film, in the framework of lubrication approximation [10, 11].

A section in the *r,z*-plane of a droplet penetrating into a porous substrate is shown in **Fig. 1**. This paper considers axisymmetric configurations ($\partial/\partial\varphi = 0$), although the theoretical model also covers three-dimensional configurations. The liquid is assumed incompressible with constant density ρ, dynamic viscosity μ, and surface tension σ. On the surface of the porous substrate, the liquid forms a macroscopic contact angle θ_e. The dynamics of a flat droplet can be described by lubrication approximation, with the evolution equation for the droplet profile, h, given by:

$$\frac{\partial h}{\partial t} - \frac{1}{3\mu}\nabla_s \cdot \left(h^3 \nabla_s p\right) = u_{pz}\big|_{z=0}, \qquad (1)$$

[10], with ∇_s denoting here the two-dimensional nabla operator and u_{pz} the volume flow rate per unit area into the substrate (at $z = 0$). The pressure term:

$$p = \rho g h - \sigma \nabla_s^2 h - \Pi_c \qquad (2)$$

for the fluid pressure p in the droplet above the porous substrate contains the influence of gravitation (with the gravitational constant g), capillary pressure, and intermolecular forces. The disjoining pressure Π_c is given by:

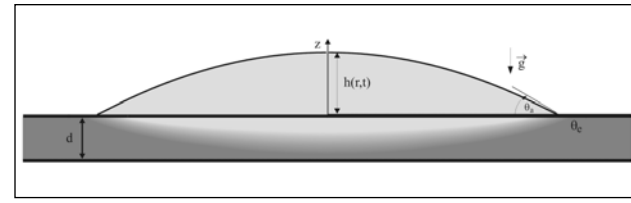

1. Spreading of a droplet on a porous substrate.

$$\Pi_c(h) = \frac{\sigma\theta_e^2}{h^*}\left(\left(\frac{h^*}{h}\right)^3 - \left(\frac{h^*}{h}\right)^2\right), \qquad (3)$$

It is used here heuristically, together with the concept of a thin precursor film h^*, to model wetting and dewetting phenomena [25]. The precursor film/disjoining pressure concept originally devised for impermeable substrates is taken over in this paper heuristically to model a macroscopic equilibrium contact angle θ_e and a moving contact line on a porous substrate. A droplet placed on an impermeable substrate with a steeper apparent contact angle θ_a will start to spread until it approaches the equilibrium contact angle θ_e in the stationary limit, with the equilibrium height h_e and contact radius R_e of the droplet. The spreading rate follows Tanner's law of spreading and the disjoining pressure, Eq. 3, determines θ_e and the contact line position [25]. The precursor film/disjoining pressure approach has a key advantage. The contact line does not enter the problem as moving boundary condition, with all its mathematical implications; rather, its position results directly from the solution of the thin film equation, extended by the disjoining pressure term. On a porous substrate, the spreading process interacts with the absorption into the porous medium. A higher equilibrium contact angle, for instance, implies smaller contact area and delays absorption, resulting in larger total sorption times or even contact line pinning at localized poorly wetting patches [10, 26]. For this paper, we chose an equilibrium contact angle $\theta_e = 10°$ and a precursor film thickness $h^* = 0.05\, h_e$.

The flow in the porous layer is considered unsaturated and governed by Richards' equation,

$$\frac{\partial c}{\partial t} = \nabla \cdot \left(\frac{k}{\mu}\nabla p_p\right), \qquad (4)$$

for the pressure p_p inside the pores of the substrate [20], with ∇ denoting the (three-dimensional) nabla operator. The volumetric fluid content of the porous medium, c, which occurs on the left hand side of Eq. 4, is defined as volume of fluid per bulk volume, taken over a representative volume. The porous medium is characterized phenomenologically by a sorption

curve $c = c\,(p_p)$, relating the fluid content, c, to the pressure, p_p, and by a saturation dependent permeability tensor, k = k(c), which is decomposed here into a product of the (scalar) relative permeability k_{rel}(c) and the anisotropy tensor k_a which accounts for an anisotropic medium,

$$\mathbf{k} = k_{rel}(c)\mathbf{k}_a \ . \tag{5}$$

It is assumed that the scalar function $k_{rel}(c)$ depends on the fluid content c, while the tensor k_a is assumed to be independent of the fluid content [20]. For the axisymmetric case ($\partial/\partial\varphi = 0$) the permeability tensor $k_a = (k_{ij})_a$ is characterized by a vertical permeability k_z and a lateral permeability k_r, i.e., $k_{rr} = k_r$, $k_{\varphi\varphi} = k_r$, $k_{zz} = k_z$, $k_{ij} = 0$, for i ≠ j, ($i, j = r, \varphi, z$).

The van Genuchten-Mualem model for the sorption curve,

$$c(p_p) = \begin{cases} c_r + \dfrac{c_s - c_r}{(1 + |\alpha\, p_p|^n)^m}, & p_p < 0 \\ c_s, & p_p \geq 0 \end{cases} \tag{6}$$

is widely used to characterize porous materials, for example, in soil science [27]. The residual fluid content c_r, the saturation content c_s, and the model parameters α, m, and n in Eq. 6 depend on the material properties of the porous medium and have to be determined by sorption experiments. Such experiments essentially imply the solution of an inverse problem [28]. Several experimental methods to determine the sorption curves $c\,(p_p)$ and the relative permeability $k_{rel}(c)$ for compact blocks of porous material are described in [20]. In [14], absorption into coated paper samples is measured directly by a Bristow absorption wheel. A device for gravimetric determination of fluid imbibition into compacted coating pigments, as used in paper coating applications, is described by Schoelkopf et al. [8]. This method appears to be a promising tool for determining the model parameters of Eq. 6 experimentally.

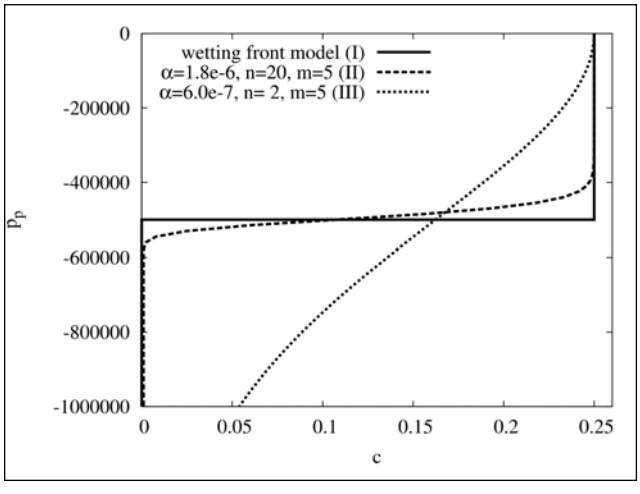

2. Sorption curves I–III: Dependence of capillary pressure p_p on saturation c (c_r = 0, c_s = 0.25).

Figure 2 illustrates some (dimensionless) sorption curves described by Eq. 6. For a wetting front model, corresponding to a sharp transition from saturated to dry regions in the porous medium [12], the sorption curve becomes a step function (curve I). The roman numbers I–III in Fig. 2 refer also to the substrate materials characterized by the sorption curves.

The relative permeability $k_{rel}(c)$ depends on the fluid content. Here, the expression

$$k_{rel}(S_e) = \sqrt{S_e}\left(1 - \left(1 - S_e^{1/m}\right)^m\right)^2 , \tag{7}$$

taken from [27], is used with the relative fluid content S_e defined as:

$$S_e(c) = \frac{c - c_r}{c_s - c_r} \ , \tag{8}$$

and with c_r, c_s, and m taken over from Eq. 6. **Figure 3** shows $k_{rel} = k_{rel}(c)$ for various values of m. The saturation dependence of the permeability reflects the fact that at low fluid content, c, smaller pores fill first because of higher capillary suction but have lower permeability [20]. Thus, the sorption curve, Eq. 6, and the relative permeability, Eq. 7, are closely interrelated functions that characterize the fluid transport in the porous medium. In the limit $c \longrightarrow c_s$, the relative permeability k_{rel} tends to 1 and the partial derivative of c with respect to time on the left hand side of Eq. 4 vanishes. Richards' equation then reduces to Darcy's law for fully saturated flow in porous media with constant (possibly anisotropic) permeability.

Equations 1 and 4 have to be coupled by appropriate interface conditions on the substrate surface: Across the substrate surface the pressure is continuous under the contact area of the droplet delimited by the contact radius $R_c(t)$:

$$p_p(r,0,t) = p(r,t), \ \text{for} \ \ r < R_c \tag{9}$$

Beyond that contact area, for $r > R_c$, the surface is assumed impermeable. The vertical sorption velocity on the substrate surface, $u_{pz}(r, 0, t)$, appearing on the right side of Eq. 1, is given by Darcy's law:

$$u_{pz} = -\frac{k_z}{\mu}\left.\frac{\partial p_p}{\partial z}\right|_{z=0} \tag{10}$$

Equation 1 is a thin film equation corresponding to a no-slip condition on the substrate, i.e., $u(r, 0, t) = 0$ holds for the horizontal velocity component of the fluid above the substrate. On impermeable boundaries of the porous substrate, the nor-

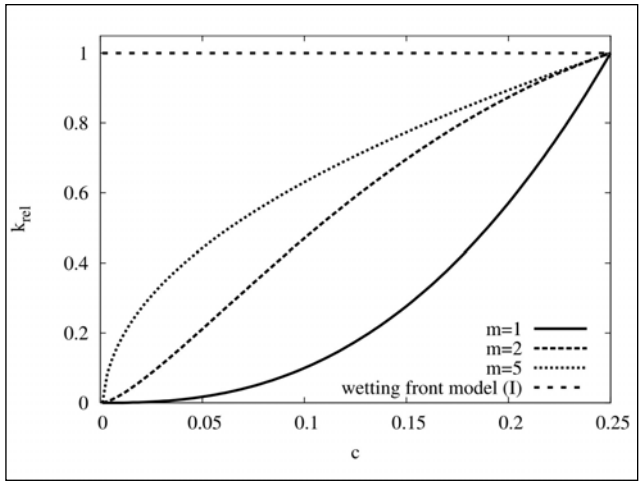

3. Dependence of relative permeability k_{rel} on saturation c, for different values of m (c_r = 0, c_s = 0.25).

mal derivative of the pressure vanishes:

$$\frac{\partial p_p}{\partial n} = 0 \qquad (11)$$

The governing equations and boundary conditions are made dimensionless by scaling the droplet height by h_e and the coordinates r, z by R_e. With these scales, the characteristic time scale is $T = 3\mu R_e^4/(\sigma h_e^3)$. The influence of gravitation shows up in the Bond number $Bo = \rho g R_e^2/\sigma$, whereas the properties of the porous substrate appear in the permeability number $Pm = 3k_z R_e^2/h_e^4$, with the vertical permeability, k_z, and the suction number $Su = p_c R_e^2/\sigma h_e$, with a capillary suction, $p_c > 0$, to be viewed as measure for the mean pore diameter [10].

RESULTS AND DISCUSSION

Numerical results are presented for spreading and sorption of axisymmetric droplets on substrate layers of thickness d, which are characterized by the three different sorption curves plotted in Fig. 2. For the step function, curve I in Fig. 2, with the transition from completely saturated to completely unsaturated conditions taking place discontinuously at $p_p = -Su = -5\times10^5$, the wetting front model [12] was used for the numerical computations. For the substrates with broader pore size distribution, as characterized by curves II and III in Fig. 2, Richards' equation (Eq. 4), coupled via Eqs. 9–10 with the evolution equation for the droplet profile, Eq. 1, is solved numerically. The remaining material properties are taken from a configuration investigated in [12], with the porosity $\phi = 0.25$, the permeability number $Pm = 10^{-5}$, and the anisotropy ratio $\kappa = k_z/k_r = 1$. For small droplet volumes, as used in ink jet applications, the influence of gravitation can be neglected, i.e., $Bo \approx 0$. The saturation fluid content, c_s, is equal to the porosity: $c_s = \phi$. These parameters could characterize a droplet volume of about 50 pL (ρ = 1000 kg/m^3, μ = 5 mPas, σ = 30 mN/m), and a (nano-)porous material with an (average) pore diameter of about 10 nm. The timescale of absorption, T, would for this case be about 50 ms.

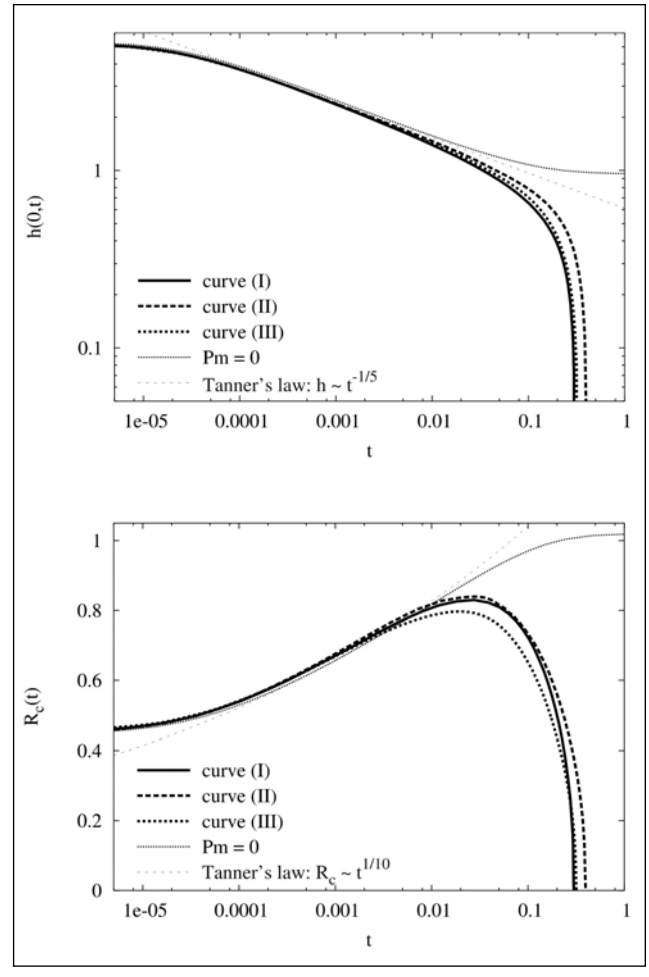

4. Sorption of a droplet into a single porous layer (d = 0.5). Droplet height h(0, t) (a) and contact radius $R_c(t)$ (b) in time dependence for sorption curves I–III: c_r = 0, c_s = 0.25, Pm = 10^{-5}, Su = 5 x 10^5, Bo ≈ 0.

Figure 4 shows the evolution of the central height $h(0, t)$ and contact radius $R_c(t)$ of the droplet, i.e., the position of the contact line, on substrate layers of thickness d = 0.5. Here it is assumed that the droplet has a steeper apparent contact angle $\theta_a > \theta_e$ when it is placed onto the substrate at t = 0. To reach its equilibrium contact angle θ_e, the droplet starts to spread, i.e., its contact radius increases while its height decreases with time. As long as $t < 0.01$, the mass loss of the droplet due to absorption of the fluid into the porous substrate is not yet significant. The spreading kinetics follows approximately Tanner's law for all three configurations shown here, as for a droplet spreading on an impermeable substrate (Pm = 0), for which the equilibrium configuration $h(0, t \longrightarrow \infty) = 1$ and $R_c(t \longrightarrow \infty) = 1$ would be reached. However, because the fluid absorbs into the porous layer, the droplet volume decreases significantly for $t > 0.01$. The equilibrium con-

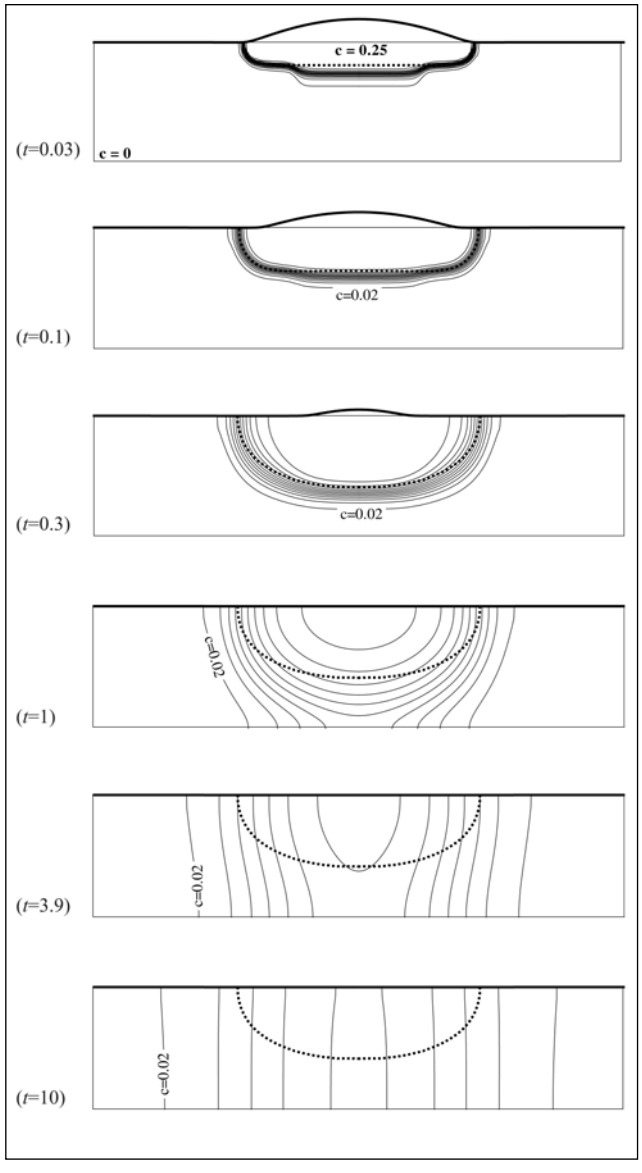

5. Droplet profiles h(r, t) (line) and fluid content c(r, t) in the porous layer (d = 0.5) at different times t as contour plot for curve II of Fig. 2, Pm = 10^{-5}, Su = 5 x 10^{5}, Bo ≈ 0. Results for the wetting front model (curve I) are shown as dashed line.

tact angle is reached earlier, compared with a droplet on an impermeable substrate, and the contact radius reaches a local maximum around $R_c \approx 0.8$ (Fig. 4b). The contact line recedes until the droplet has been absorbed.

The sorption curve II in Fig. 2 has a narrow transition from the fully saturated state of the porous medium ($c = c_s = 0.25$) to the completely unsaturated state ($c = c_r = 0$), localized around $p_p = -5 \times 10^5$. This smooth transition of the sorption curve corresponds to a transition region of finite extent from fully saturated to completely unsaturated regions in the porous layer, which delays the sorption process, as the evo-

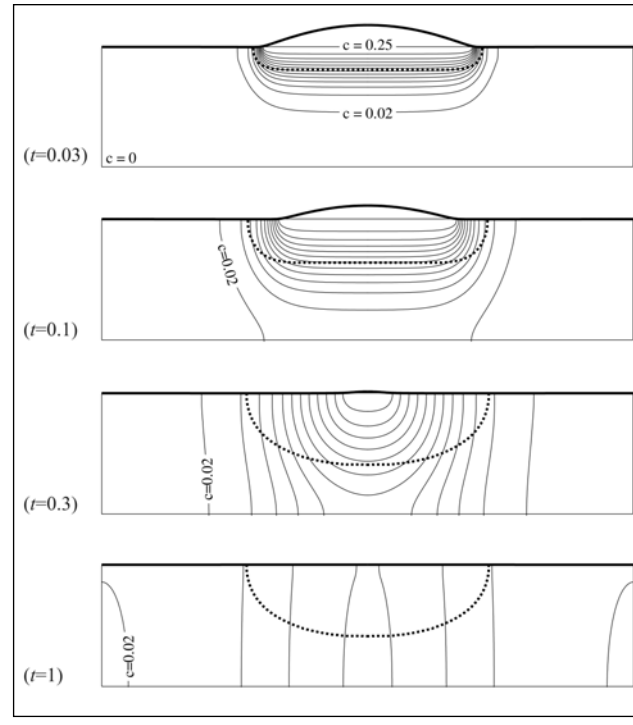

6. Droplet profiles h(r, t) (line) and fluid content c(r, t) at different times t in the porous layer (d = 0.5) as contour plot for curve III of Fig. 2, Pm = 10^{-5}, Su = 5 x 10^{5}, Bo ≈ 0. Results for the wetting front model (curve I) are shown as dashed line.

lution of the droplet profile indicates. Compared with the absorption time for the wetting front model (curve I), $t_{s,I} \approx 0.3$, the absorption time for the medium characterized by the smooth sorption (curve II) is 30% larger: $t_{s,II} \approx 0.4$. Curve III in Fig. 2 represents a broad transition that extends far into the region of negative pressures, $p_p << -Su$. This sorption curve characterizes a material with a large fraction of very small pores and high capillary suction. The suction of these small pores apparently enhances the penetration of the fluid (see Fig. 4) and compared with material (curve II) reduces the time for total absorption to $t_{s,III} \approx 0.32$. The results indicate that the macroscopic model for unsaturated flow, using a phenomenological sorption curve, appears to capture, at least qualitatively, the microscopic absorption mechanism in pore networks described in [18]. The results also imply that two different pore size distributions, a uniform pore size described by the wetting front model (curve I) on the one hand and a broad pore size distribution described by curve III on the other hand, may give comparable absorption times for the droplet. Also, the absorption times for the droplets, t_s, denote just the end of phase 1 spreading, while inside the porous medium significant unsaturated fluid transport, phase 2 spreading [19], will take place for $t > t_s$.

To get better insight into the fluid distribution in the porous layers, the volumetric fluid content, c, is shown in **Figs. 5** and

6 as contour plot for different time steps, together with the droplet profile and the location of the wetting front, computed according to [12]. The same equidistant contour levels (Δc = 0.02) for all contour plots are used in Figs. 5 and 6.

For a porous material with the (narrow) sorption curve II, the transition from saturated ($c = c_s$) to completely unsaturated ($c = c_r$) regions in the porous layer is also narrow as long as the droplet on the substrate surface is not yet completely absorbed ($t < 0.3$), see Fig. 5. During this period (phase 1 sorption), the location of the wetting front, as computed for material I by the wetting front model [12], is accurate within this transition region. Similarly, good agreement was found among numerical results of the wetting front model for phase 1 spreading of a liquid stain in a thin porous layer and experimental results of Borhan and Rungta [29] in [12]. As soon as the droplet is absorbed completely, the advance of the sharp wetting front stops due to mass conservation. However, for unsaturated flow, phase 2 sorption sets in and the initially narrow transition region of the fluid content c broadens while the fluid fills the pores in the layer partially, $c_r < c < c_s$. During this process, the fully saturated regions are gradually depleted. For $0.3 < t < 1$ the fluid penetrates vertically, until it reaches the impermeable bottom. Sorption with almost vertical contour lines of c, characteristic for radial sorption as observed in thin substrates by [19], takes place for $t >> 1$. Although the fluid penetrates far beyond the region delimited by the wetting front model and reaches even the bottom of the porous layer, a significant part of the fluid stays below the area delimited by the maximum radial extent of the wetting front.

The broad sorption curve III of Fig. 2 changes the picture qualitatively as the contours for the fluid content c in Fig. 6 indicate. In the initial stages of spreading and sorption, the fluid penetrates significantly deeper into the porous layer than predicted by the wetting front model. At $t = 0.1$ a small fraction of fluid reaches the impermeable bottom and starts to penetrate radially, as in unsaturated flow with $c_r < c < c_s$. When the droplet volume has almost disappeared, at $t = 0.3$, the fluid partially fills the layer across its entire depth under the area marked by the maximum radial extension of the droplet. Outside this area, radial penetration, with almost vertical contours of the fluid content can be seen. For $t = 1$, almost all the domain is partially filled with fluid ($c_r < c < c_s$), which spreads like a coffee stain on paper or textiles.

The numerical results show that the wetting front model can describe phase 1 sorption into materials that are characterized by sorption curves with a narrow transition from fully saturated to the unsaturated state. Such materials provide sharp localization of the imbibed fluid during phase 1 sorption, i.e., a small dot size for high printing resolution. This property makes them suitable for high-resolution ink jet applications, especially when immobilisation of the ink by drying or solidification can be matched to coincide with the end of phase 1 sorption and avoid further increase of the fluid

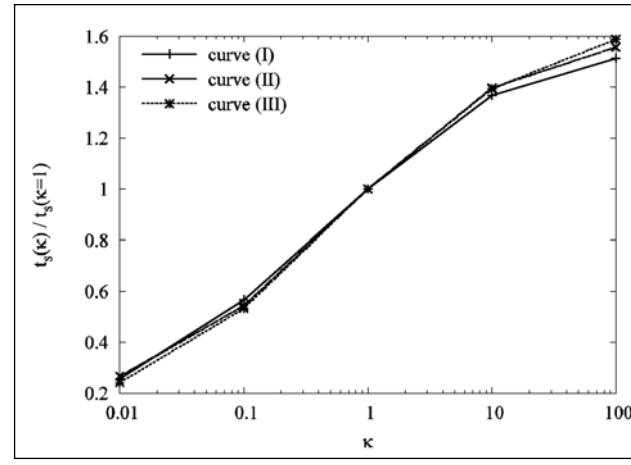

7. Influence of layer anisotropy ratio on sorption time. Normalized sorption time $t_s(\kappa)/t_s(\kappa=1)$ vs. anisotropy ratio κ.

covered area during phase 2 sorption, as indicated in Fig. 5 for $t > 0.3$. Although the sorption characteristic of curve III favors rapid absorption, the fluid penetrates into a larger volume of the porous layer and results in coarser resolution and possibly blurred contours in printing. The process of phase 2 sorption, shown in Fig. 6 between $t = 0.3$ and $t = 1$, occurs roughly an order of magnitude faster, as compared with similar local fluid distributions in Fig. 5 between $t = 3.9$ and $t = 10$. Therefore, faster deterioration of printing resolution will be expected for a curve III material.

Figure 7 shows the influence of the anisotropy ratio κ (for fixed value of k_z) on the sorption time $t_s(\kappa)$ for complete absorption of the droplet, normalized with the sorption time for the isotropic case, κ=1. The relative change of the sorption time with the anisotropy ratio appears to be essentially independent of the sorption curve. For dominant vertical sorption, i.e., for $k_z >> k_r$, the sorption time increases by about 50%–60%, which was also found for the limiting case $k_r \longrightarrow 0$ of the wetting front model [10, 12]. With increasing lateral permeability, $k_z < k_r$, the sorption time decreases. A high lateral permeability enhances droplet absorption and decreases the penetration depth of the fluid, which favors fast printing on thin receiver layers. However, the resolution, for a given droplet volume, may be significantly coarser because of the larger covered area [12].

Finally, the influence of porous layer thickness on the sorption kinetics has been investigated for the three different sorption curves of Fig. 2. In **Fig. 8a**, the behavior of the wetting front model (curve I) on substrates of thicknesses d = 0.5 and $d = 0.25$, respectively, is plotted in terms of the evolution of the contact radius $R_c(t)$, together with the sorption kinetics on curve II layers. For the wetting front model, the front hits the impermeable bottom at $t_{bot,I,0.25} \approx 0.2$ for d = 0.25, while for $d = 0.5$ it does not reach it at all (Fig. 5). As described in [12], the pressure gradients in the porous layer de-

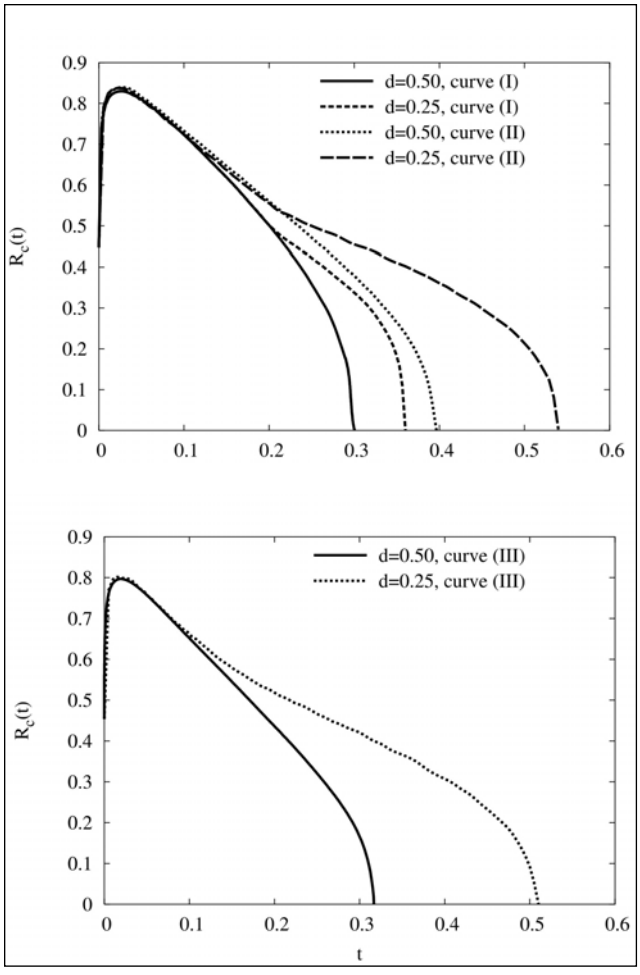

8. Influence of layer thickness d and sorption characteristics on droplet sorption kinetics. (a) Evolution of contact radius $R_c(t)$ for wetting front model (curve I) and sorption (curve II) on substrate layers with thickness d = 0.5 and d = 0.25, respectively. (b) Same for material III. c_r = 0, cs = 0.25, Pm = 10^{-5}, Su = 5 x 10^5, Bo ≈ 0.

crease for preferentially radial suction ($t > t_{bot}$) and the retraction of the contact line is delayed, so that the total absorption time increases by about 20%, to $t_{s,I,0.25}$≈0.36. Similar behavior is seen in a substrate characterized by sorption curve II. Here, the interaction of the penetrating fluid with the impermeable bottom for d = 0.25 becomes dominant for t > 0.22, as seen also in Fig. 8, and the total sorption time increases by about 35% to $t_{s,II,0.25}$≈0.54.

Fig. 8b shows the influence of the layer thicknesses on the sorption kinetics of a droplet on a porous material characterized by curve III. Due to the broad transition region of unsaturated flow, the interaction with the impermeable bottom of the layer sets in significantly earlier, at t > 0.1. The total sorption time increases by about 60%, when the layer thickness is reduced from d = 0.5 to d = 0.25. The total sorption

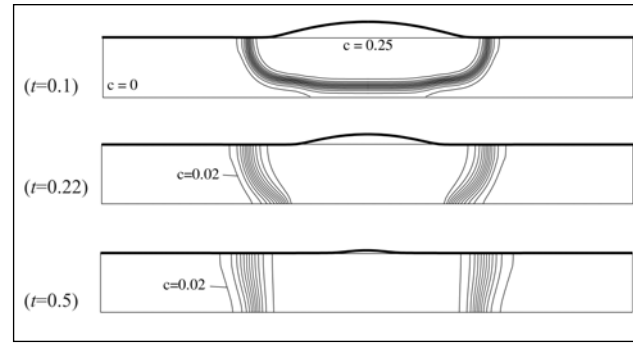

9. Droplet profiles h(r, t) (line) and the fluid content c(r, t) in a porous layer of thickness d = 0.25 for material II at different times t as contour plot. Pm = 10^{-5}, Su = 5 x 10^5, Bo ≈ 0.

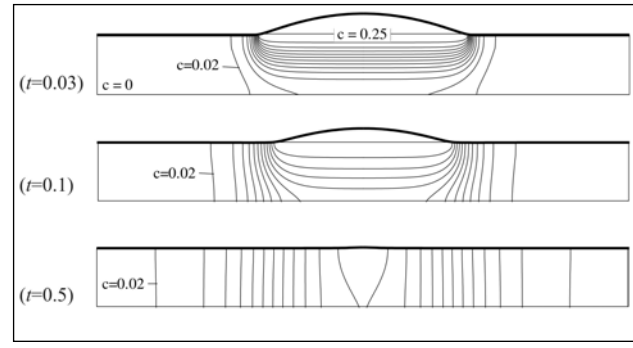

10. Droplet profiles h(r, t) (line) and fluid content c(r, t) in porous layer of thickness d = 0.25 for material II) at different times t as contour plot. Pm = 10^{-5}, Su = 5 x 10^5, Bo ≈ 0.

time on the thinner substrate (d = 0.25), $t_{s,III,0.25}$ ≈0.51, approaches $t_{s,II,0.25}$ ≈ 0.54 of material II, so that for d = 0.25 the two substrate materials differ little as the total sorption time is considered. However, for d = 0.5 there is a significant difference, $t_{s,II}$ ≈ 0.4 compared with $t_{s,III}$ ≈ 0.32. **Figs. 9** and **10** show the fluid distribution in the porous layer at different time steps. For t = 0.5 the fluid has moved already further in radial direction in material III than in material II.

The computations show that the thickness of the ink receiving layer may influence the process speed of an ink-jet process by delaying the droplet absorption significantly as soon as the fluid reaches the layer's bottom boundary. To achieve rapid absorption for high speed printing, the layer thickness has to match the volume of the impinging droplets.

CONCLUSIONS

For ink-jet applications, the numerical results imply that porous ink receiving layers with a steep sorption curve allow for the application of sharply localized dots. Because continuing fluid migration after complete droplet absorption will lead to coarser and blurred dots, immobilization of the ink should coincide closely with the end of phase 1 sorption.

Further, the thickness of the receiving layer has to match the droplet volume to avoid interaction of the penetrating fluid with the (impermeable) bottom of the receiving layer, which can significantly delay the droplet absorption and reduce process speed. **TJ**

ACKNOWLEDGMENT

This work was supported by the German Research Foundation (DFG).

Submitted: December 21, 2005
Revised: November 3, 2006
Accepted: November 5, 2006

LITERATURE CITED

1. Alleborn, N., Raszillier, H., Lievens, O., et al., *5th European Coating Symposium Proceedings*, Polytype Converting, Fribourg, Switzerland, 2004, pp. 246–251.
2. Clarke, A., Blake, T.D., Carruthers, K., et al., *Langmuir* 18(8): 2980(2002).
3. Desie, G., Allaman, S., Lievens, O., et al., *International Conference on Digital Printing Technologies Proceedings*, Vol. 18, Society for Imaging and Technology, San Diego, California, USA, 2002, pp. 360–365.
4. Holman, R.K., Cima, M.J., Uhland, S.A., et al., *J. Coll. Interface Sci.* 249(2): 432(2002).
5. Bousfield, D.W., *Tappi J.* 74(5): 163(1991).
6. Sünderhauf, G., Raszillier, H., and Durst, F., *Advances in Coating and Drying of Thin Films: 3rd European Coating Symposium Proceedings*, Shaker-Verlag, Aachen, Germany, 1999, pp. 163-168.
7. Toivakka, M.O. and Bousfield, D.W., *J. Pulp Pap. Sci.* 25(5): 183(1999).
8. Schoelkopf, J., Ridgway, C.J., Gane, P.A.C., et al., *J. Colloid Interface Sci.* 227(1): 119(2000).
9. Alleborn, N., Durst, F., and Lienhart, F., *Chem. Ing. Tech.* 77(1–2): 84(2005).
10. Alleborn, N. and Raszillier, H., *Chem. Eng. Sci.* 59(10): 2071(2004).
11. Davis, S.H. and Hocking, L.M., *Phys. Fluids* 11(1): 48(1999).
12. Alleborn, N. and Raszillier, H., *J. Colloid Interface Sci.* 280(2): 449(2004).
13. Starov, V.M., Velarde, M.G., and Zhdanov, S.A., *J. Colloid Interface Sci.* 252(2): 397(2002).
14. Bousfield, D.W. and Karles, G., *J. Colloid Interface Sci.* 270(2): 396(2004).
15. Schoelkopf, J., Gane, P.A.C., Ridgway, C.J., et al., *Nord. Pulp Pap. Res. J.* 15: 422(2000).
16. Ridgway, C.J., Schoelkopf, J., Matthews, G.P., et al., *J. Colloid Interface Sci.* 239(2): 417(2001).
17. Schoelkopf, J., Gane, P.A.C., and Ridgway, C.J., *Colloids Surf. A: Physicochem. Eng. Aspects* 236(13): 111(2004).
18. Ridgway, C.J., Gane, P.A.C., and Schoelkopf, J., *Colloids Surf. A: Physicochem. Eng. Aspects* 236(1–3): 91(2004).
19. Gillespie, T., *J. Colloid Sci.* 13: 32(1958).
20. Bear, J., *Dynamics of Fluids in Porous Media*, Dover, New York, USA, 1988.
21. Kumar, S.M. and Deshpande, A.P., *Colloids Surf. A: Physicochem. Eng. Aspects* 277(1–3): 157(2006).
22. Zadrazil, A., Stepanek, F., and Matar, O.K., *J. Fluid Mech.* 562: 1(2006).
23. Alleborn, N. and Raszillier, H., Unsaturated sorption of films and droplets spreading on porous substrates, *6th European Coating Symposium Proceedings*, University of Bradford, UK, 2005.
24. Alleborn, N. and Raszillier, H., *2006 TAPPI Advanced Coating Fundamentals Symposium Proceedings*, TAPPI Press, Atlanta, Georgia, USA, pp. 177–190.
25. Schwartz, L.W. and Eley, R.R., *J. Colloid Interface Sci.* 202(1): 173(1998).
26. Alleborn, N. and Raszillier, H., *5th European Coating Symposium Proceedings*, Polytype Converting, Fribourg, Switzerland, 2004, pp. 261–266.
27. Simunek, J., Vogel, T., and van Genuchten, M.Th., in "The SWMS_2D code for simulating water flow and solute transport in two-dimensional variably saturated media," Research report no. 132, U.S. Department of Agriculture, Washington, DC, USA, 1994.
28. Bitterlich, S. and Knabner, P., *J. Comput. Appl. Math.* 147(1): 153(2002).
29. Borhan, A. and Rungta, K.K., *J. Colloid Interface Sci.* 158(2): 403(1993).

INSIGHTS FROM THE AUTHORS

Alleborn

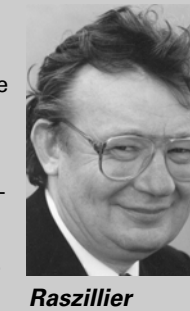

Raszillier

Our research group has been looking at capillary hydrodynamics of thin liquid films and droplets. We were interested in ink jet printing applications. The work presented here goes far beyond previous research on spreading of droplets on porous substrates using conventional wetting front models. The challenge was to extend the wetting front model to describe continuous transition from completely saturated to completely unsaturated parts of the porous layer and couple it numerically with film or droplet dynamics.

It is particularly interesting that different pore size distributions may result in similar absorption times and the finite layer thickness may have a strong influence on sorption time. The numerical models give an insight into how substrate properties such as thickness, sorption curves, and pore sizes may influence absorption kinetics of films or droplets. Various scenarios for different configurations of the ink receiving layers can be investigated numerically before extensive laboratory experiments or pilot plant trials.

Our next step will be to include inertia effects on the impinging droplet.

Alleborn is a scientist at the University Erlangen-Nürnberg, Erlangen, Germany. Raszillier is a senior scientist, retired from the University Erlangen-Nürnberg, Erlangen, Germany; email Alleborn at alleborn@lstm.uni-erlangen.de